BILINGUAL PUBLISHING GROUP

Journal of Environmental & Earth Sciences

https://journals.bilpubgroup.com/index.php/jees

ARTICLE

Comparative Study of MnO_2 and Fe_2O_3 Composites on *Toona ciliata*–Derived Carbon for Sustainable Supercapacitor Applications

Dibyashree Shrestha

Department of Chemistry, Institute of Science and Technology, Patan Multiple Campus, Tribhuvan University, Kathmandu, Bagmati 44600, Nepal

ABSTRACT

Unmanaged wood waste, particularly in countries like Nepal, presents serious environmental concerns due to open burning and improper disposal, leading to carbon emissions, air pollution and land degradation. This study introduces an environmentally sustainable strategy to upcycle *Toona ciliata* wood scrap—an abundant and underutilized lignocellulosic biomass—into high performance carbon electrodes for green energy storage applications. Activated carbon (TCWAC) was synthesized via single-step pyrolytic carbonization followed by phosphoric acid activation, yielding a material with high specific surface area, hierarchical porosity, and excellent electrical conductivity. Electrochemical measurements using a three-electrode configuration in 6 M KOH revealed optimized potential windows of –1.0 to –0.2 V (TCWAC), –1.2 to 0 V (TCWAC–Mn), and –1.15 to –0.4 V (TCWAC–Fe). TCWAC exhibited a specific capacitance of 156.3 Fg^{-1} at 1 Ag^{-1}, with an energy density of 3.5 $Whkg^{-1}$, and 80.2% capacity retention after 1000 charge–discharge cycles. Composites with MnO_2 and Fe_2O_3 were also evaluated. TWAC-Mn delivered 489.4 Fg^{-1}, 25.1 $Whkg^{-1}$, and 99.1% retention, whereas, TWAC-Fe achieved 321.3 Fg^{-1}, 6.3 $Whkg^{-1}$, and 90.3% retention. The superior performance of MnO_2 is attributed to its multiple oxidation states, facilitating reversible faradaic redox and enhanced pseudocapacitance. This work offers the first direct, systematic comparison of MnO_2 and Fe_2O_3 composites on a common biomass-carbon matrix under identical synthesis and testing conditions. The finding provides mechanistic insight into charge storage behaviour and demonstrate a scalable route for converting biomass waste into sustainable electrode materials, contributing to cleaner energy solutions and improved biomass valorization.

Keywords: *Toona ciliata* Wood Scrap; Activated Carbon Electrodes; Supercapacitor; MnO_2 Composites; Fe_2O_3 Composites; Sustainable Energy Storage

*CORRESPONDING AUTHOR:

Dibyashree Shrestha, Department of Chemistry, Institute of Science and Technology, Patan Multiple Campus, Tribhuvan University, Kathmandu, Bagmati 44600, Nepal; Email: shresthadibyashree@gmail.com

ARTICLE INFO

Received: 3 June 2025 | Revised: 24 June 2025 | Accepted: 30 June 2025 | Published Online: 7 July 2025

DOI: https://doi.org/10.30564/jees.v7i7.10332

CITATION

Shrestha, D., 2025. Comparative Study of MnO_2 and Fe_2O_3 Composites on Toona ciliata–Derived Carbon for Sustainable Supercapacitor Applications. Journal of Environmental & Earth Sciences. 7(7): 240–259. DOI: https://doi.org/10.30564/jees.v7i7.10332

1. Introduction

The global shift toward sustainable and efficient energy storage has intensified the demand for environmentally friendly electrode materials. Among various alternatives, activated carbons derived from biomass have gained considerable attention for supercapacitor applications due to their natural abundance, low cost, high surface area, and tunable porosity [1,2]. However, these biomass-derived carbons often exhibit limited electrical conductivity and involve complex activation steps, which can hinder their scalability. Therefore, identifying underutilized biomass sources with favorable physicochemical properties and developing scalable processing routes are critical for advancing green energy systems.

Wood waste, when mismanaged, leads to environmental degradation through open burning and landfill accumulation. In South Asia, particularly Nepal, the lack of recycling infrastructure, widespread open dumping, and unsustainable disposal practices exacerbate this issue. These actions contribute significantly to carbon emissions, land degradation, and air pollution, posing threats to both environmental and public health. Upcycling such biomass waste into energy storage materials supports sustainable resource use, reduces environmental burden, and offers a pathway for cleaner energy recovery from underutilized biomass.

Energy storage technologies are essential across multiple sectors, including portable electronics, electric vehicles, and renewable energy systems. Among them, supercapacitors (also known as environmental energy capacitors) have emerged as promising devices due to their high power density, rapid charge–discharge capability and long cycle life. Bridging the gap between batteries and conventional capacitors, supercapacitors offer faster energy delivery than batteries and store more energy than standard capacitors. Based on the charge storage mechanism, supercapacitors are categorized into electric double-layer capacitors (EDLCs), which rely on electrostatic ion adsorption, and pseudocapacitors, which store energy via fast faradaic redox reactions. Hence selecting and eco-designing suitable electrode materials are crucial for improving supercapacitor performance and enabling practical, sustainable applications [3–5].

Unlike many prior reports that utilize multi-step, energy-intensive activation or expensive templating approaches, the present study introduces a simplified, single-step carbonization combined with phosphoric acid activation to produce activated carbon with highly accessible porous networks. This eco-friendly synthesis not only reduces processing complexity but also facilitates scalable production of high-performance biomass-derived carbons suitable for supercapacitor electrodes**.**

This study investigates *Toona ciliata* wood scrap—locally known as "Tuni" in Nepal—as a renewable, low-cost, and underutilized biomass precursor for activated carbon production. *Toona ciliata* is a fast-growing hardwood widely used in carpentry and construction, generating substantial wood waste that is often discarded or burned, thereby worsening Nepal's biomass waste burden. The proposed strategy aligns with regional environmental priorities in South Asia, emphasizing low-carbon technologies and biomass valorization for energy solutions.

While both MnO_2 and Fe_2O_3 have been extensively studied individually as pseudocapacitive materials, the majority of reported studies employ different biomass sources, preparation methods, or test protocols, which complicates direct performance comparisons. This study addresses this gap by systematically comparing MnO_2 and Fe_2O_3 composites fabricated on an identical *Toona ciliata*-derived activated carbon matrix (TCWAC), under fully comparable synthesis routes, identical mass loading, and uniform electrochemical testing conditions. This direct head-to-head comparison offers mechanistic understanding of how distinct redox kinetics and ion transport behaviors contribute to their relative performance differences, which is rarely explored in biomass-carbon based electrode systems.

A single-step carbonization process with H_3PO_4 activation was used to synthesize activated carbon (TCWAC) featuring high surface area and well-developed porosity, making it ideal for supercapacitor applications. In addition, through careful tuning of the synthesis parameters, a unique hierarchical pore architecture combining micro- and mesopores was achieved, ensuring efficient ion transport and electrolyte accessibility critical for high-rate performance. To enhance electrochemical performance, TCWAC was composited with manganese dioxide (MnO_2) and iron(III) oxide (Fe_2O_3), introducing pseudocapacitive

behavior via synergistic redox activity. Comprehensive characterization techniques—including SEM, TEM, BET, XRD, Raman, FTIR, and XPS—were employed to analyze morphology, surface chemistry, and structural features, thereby supporting the interpretation of the electrochemical results. Additionally, advanced electrochemical impedance spectroscopy (EIS) was conducted to extract key kinetic parameters such as charge transfer resistance and ion diffusion, providing deeper mechanistic insights into the electrode–electrolyte interface behavior of these hybrid composites.

Key Contributions of This Study

- **Sustainable Conversion of *Toona ciliata* Wood Waste: Scalable single-step synthesis of functional energy materials**

This study proposes an eco-friendly and streamlined one-step carbonization-activation method to convert *Toona ciliata* wood scrap into biomass-derived energy materials for green supercapacitor systems, addressing both waste management and clean energy needs.

- **Development of High-Performance TCWAC–Metal Oxide Composites:**

TCWAC was successfully integrated with MnO_2 and Fe_2O_3, resulting in enhanced-specific capacitance, energy density, and cycling stability due to synergistic redox behavior.

- **Direct Comparative Analysis:**

This is the first study to directly compare MnO_2- and Fe_2O_3-based TCWAC composites under identical conditions, demonstrating the superior eco-capacitive performance of the MnO_2 composite. The direct comparative approach provides valuable mechanistic understanding rarely available in existing literature.

These findings contribute to the rational design of sustainable hybrid electrode systems by elucidating material–property relationships that govern pseudocapacitive performance. The insights derived here can guide the future development of biomass valorization routes for scalable, high-efficiency energy storage systems.

2. Materials and Methods

2.1. Biomass Precursor

Wood scraps of *Toona ciliata* (locally known as "Tuni") were collected from carpentry workshops in Lalitpur, Nepal. These locally available, underutilized lignocellulosic residues served as a renewable biomass precursor for the sustainable recovery of carbon materials.

2.2. Eco-Materials and Reagents

The following analytical-grade reagents and materials were used throughout the study:

- **Phosphoric Acid (H_3PO_4)**: 85% concentration (15.0 M), specific gravity 1.73 g/mL; used as a green activating agent (Fischer Scientific, India Pvt. Ltd).
- **Double-Distilled Water (DW)**: used as a solvent for washing and dilution steps.
- **Carbon Black**: Battery-grade conductive additive (Sigma-Aldrich, USA).
- **Polyvinylidene Fluoride (PVDF)**: polymer binder (Sigma-Aldrich).
- **N-Methyl-2-pyrrolidone (NMP)**: Anhydrous solvent for slurry preparation (Sigma-Aldrich).
- **Nickel Foam (Ni-Foam)**: reusable current collector (PRED MATERIALS International).
- **Manganese Dioxide (MnO_2)**: ≥99% purity; used as a pseudocapacitive additive (APS Ajax Finechem, Australia).
- **Iron(III) Oxide (Fe_2O_3)**: ≥98% purity; used as a comparative additive (APS Ajax).

The *Toona ciliata* wood scraps were sourced directly as raw sawdust from the initial carpentry stage, prior to any painting or surface treatments, ensuring uncontaminated biomass for reproducible carbon synthesis.

2.3. Preprocessing of Biomass

The collected *Toona ciliata* wood scraps were air-dried and manually cleaned to remove foreign matter. This preprocessing step ensured consistent biomass quality for material development.

2.4. Preparation of Wood Powder

The dried wood scraps were crushed and ground using standard laboratory equipment. The powder was then sieved to a particle size below 100 μm to obtain a uniform

feedstock for activated carbon synthesis.

2.5. Synthesis of Activated Carbon

2.5.1. Impregnation and Drying

Twenty grams of *Toona ciliata* wood powder was mixed with phosphoric acid (H_3PO_4) at a 1:1 weight ratio. The mixture was stirred using a glass rod and immersed in approximately 100 mL of double-distilled water. The mixture was soaked at room temperature for 24 hours to facilitate acid penetration, after which the biomass was oven-dried at 110 °C for 2 hours. These synthesis conditions were selected based on preliminary trials balancing activation efficiency and preservation of porous structure while maintaining eco-friendly processing [1,5].

2.5.2. Carbonization and Washing

The dried biomass–acid mixture was carbonized in a tubular furnace at 400 °C for 3 hours under continuous nitrogen flow (100 mL/min), using a heating rate of 10 °C/min to maintain an oxygen-free environment. After natural cooling to room temperature, the carbonized product was rinsed 5–6 times with hot double-distilled water to remove residual acid and soluble by-products, followed by final washes with cold water.

The pH of the wash water was monitored after each cycle using a Hanna HI2211 pH meter (±0.01 pH accuracy) until it stabilized at a neutral value of 7.00 ± 0.05. This water-efficient washing process effectively removed residual H_3PO_4 while minimizing chemical waste and ensuring environmental safety.

2.5.3. Sample Designation

The final activated carbon product was designated as *Toona ciliata* wood scrap-derived activated carbon (TCWAC) and used in all subsequent eco-performance assessments.

2.6. Characterization of TCWAC

To assess its potential for sustainable energy storage, the structural, morphological, and surface properties of TCWAC were characterized using the following techniques:

- **X-ray Diffraction (XRD):** Performed using a RIGAKU diffractometer (Japan) to analyze phase composition and carbon crystallinity.
- **Raman Spectroscopy:** Conducted with HORIBA LabRAM HR Evolution spectrometer (Japan), to evaluate the degree of graphitization and lattice disorder via D and G band analysis.
- **Fourier Transform Infrared Spectroscopy (FTIR):** Measured with a BRUKER Vertex 70/80 spectrometer (Germany) to identify surface functional groups, particularly oxygenated species important for wettability and capacitance.
- **X-ray Photoelectron Spectroscopy (XPS):** Used a Thermo Scientific ESCALAB 250Xi system (USA), to determine surface elemental composition and chemical states contributing to pseudocapacitance.
- **BET Surface Area and Porosity Analysis:** Carried out using nitrogen adsorption–desorption isotherms on a Micromeritics ASAP 2020 analyzer (USA**)** to measure specific surface area, pore volume, and pore size distribution.
- **Scanning Electron Microscopy (SEM):** Employed a Mini SEM Nanoeyes (Korea) to observe surface morphology and pore distribution.
- **Transmission Electron Microscopy (TEM):** Utilized a JEOL JEM-2100 TEM (Japan), to examine internal microstructure and nanoscale porosity.

This multi-technique characterization provided critical insights into TCWAC's structure–property relationships and its viability as a green electrode material.

2.7. Electrode Fabrication for Sustainable Energy Storage

2.7.1. TCWAC Electrode Preparation

To prepare the working electrode, 8 mg of TCWAC, 1 mg of conductive carbon black, and 1 mg of PVDF binder were thoroughly mixed in a clean, dry mortar and pestle. The dry blend was then dispersed in 200 µL of N-methyl-2-pyrrolidone (NMP) and ground further to viscous slurry. A 70 µL aliquot of this slurry was drop-cast onto a 1 cm^2 rectangular piece of nickel foam (Ni-foam) and left to air-dry at

room temperature. The total mass loading of active material per electrode was approximately 2.8 mg cm^{-2}, calculated based on the dried mass of the 70 µL slurry containing 8 mg TCWAC, 1 mg carbon black, and 1 mg PVDF binder. This loading was measured after drying and maintained consistently across all electrode samples to ensure reproducible electrochemical performance. Ni-foam served as a lightweight, corrosion-resistant current collector [6–8].

2.7.2. Hybrid Composite Electrodes (TCWAC-Mn and TCWAC-Fe)

To explore the synergistic effects between the carbon matrix and pseudocapacitive metal oxides, TCWAC was combined with MnO_2 or Fe_2O_3 in a 1:1 weight ratio through manual grinding. The resulting materials were labeled TCWAC-Mn and TCWAC-Fe, respectively. No post-synthesis thermal treatment (e.g., calcination) was performed to preserve the porous structure of TCWAC and avoid potential collapse of its delicate hierarchical porosity. As a result, it is reasonable to assume that the BET surface areas of the composites are predominantly governed by the TCWAC matrix. Therefore, separate BET analyses for the composites were not conducted in this study. Electrodes were fabricated following the same procedure as the pristine TCWAC to ensure uniformity in coating and mass loading.

2.8. Electrochemical Performance Evaluation

The electrochemical behavior of TCWAC, TCWAC-Mn, and TCWAC-Fe electrodes was evaluated using a three-electrode setup in 6 M KOH electrolyte. A platinum wire and an Ag/AgCl (3 M KCl) electrode were used as the counter and reference electrodes, respectively. All tests were conducted at room temperature using a computer-controlled potentiostat.

2.8.1. Cyclic Voltammetry (CV)

CV was used to assess capacitive behavior and redox activity. The potential windows were optimized based on stability and charge storage characteristics of each electrode:

- **TCWAC:** −1.0 to −0.2 V
- **TCWAC–Mn:** −1.2 to 0.0 V
- **TCWAC–Fe:** −1.15 to −0.4 V

Scan rates ranged from 5 to 100 mVs^{-1}, capture both surface-controlled and diffusion-controlled processes [9].

2.8.2. Galvanostatic Charge–Discharge (GCD)

GCD measurements were performed at current densities from 1 to 10 Ag^{-1} to evaluate rate capability, coulombic efficiency, and specific capacitance. Discharge curves were used to calculate specific capacitance and compare performance under various current loads [10].

2.8.3. Electrochemical Impedance Spectroscopy (EIS)

EIS was conducted over a frequency range of 100 kHz to 0.1 Hz with a 10 mV AC perturbation. The Nyquist plots were fitted using NOVA software to extract solution resistance (Rs), charge transfer resistance (Rct), and ion diffusion behavior (Warburg impedance), providing insight into ion transport and interfacial behavior relevant to sustainable energy systems.

2.9. Replicates and Statistical Analysis

All electrochemical measurements (CV, GCD, and EIS) and BET surface area analyses were conducted in triplicate (n = 3) to ensure reproducibility. Results are reported as mean ± standard deviation (SD). One-way ANOVA was used for statistical comparison between electrode types, with $p < 0.05$ considered statistically significant. Standard deviation values are provided alongside mean values in **Tables 1–4** and discussed in Sections 3.6–3.7 (**Table 1**), Section 3.8 (**Table 2**), Section 3.9 (**Table 3**), and the overall comparative discussion in Sections 3.5–3.9 (**Table 4**).

Table 1. Specific Capacitance (Cs) of TCWAC, TCWAC-Mn, and TCWAC-Fe Electrodes at Various Current Densities. Specific Capacitance Values are Reported as Mean ± Standard Deviation (n = 3).

Current Densities (Ag^{-1})	Specific Capacitance (C_s) (Fg^{-1}, n = 3)		
	TCWAC	TCWAC-Mn	TCWAC-Fe
1	156.3 ± 1.08	489.4 ± 6.36	321.3 ± 2.80
2	138.4 ± 2.5	367.5 ± 5.2	262.4 ± 3.8
3	127.1 ± 2.1	227.9 ± 4.6	109.2 ± 2.3
5	101.3 ± 1.9	119.9 ± 2.6	86.4 ± 1.7
10	88.2 ± 1.5	110.2 ± 2.1	65.4 ± 1.3
15	55.4 ± 1.2	101.5 ± 2.4	41.0 ± 1.0
20	33.3 ± 0.9	97.4 ± 2.0	33.6 ± 0.8

Table 2. Energy Density and Power Density Values Obtained from GCD Measurements for TCWAC, TCWAC–Mn, and TCWAC–Fe electrodes. Values are Reported as Mean ± Standard Deviation (n = 3).

Electrode	Energy Density ($Whkg^{-1}$, n = 3)	Power Density (Wkg^{-1}, n = 3)
TCWAC	3.5 ± 0.17	371.4 ± 5.38
TCWAC–Mn	25.1 ± 0.72	371.4 ± 4.89
TCWAC–Fe	6.3 ± 0.26	296.2 ± 1.57

Table 3. Electrochemical Impedance Spectroscopy (EIS) Parameters for TCWAC, TCWAC–Mn, and TCWAC–Fe Electrodes (Mean ± SD, n = 3).

Parameter	TCWAC	TCWAC–Mn	TCWAC–Fe
Specific Capacitance, Cs (Fg^{-1}, n = 3)	156.3 ± 1.08	489.4 ± 6.36	321.3 ± 2.80
Series Resistance, Rs (Ω, n = 3)	0.43 ± 0.017	0.38 ± 0.017	0.41 ± 0.020
Charge Transfer Resistance, Rct (Ω, n = 3)	0.173 ± 0.025	0.110 ± 0.005	0.143 ± 0.010
Warburg Impedance, W (Ω, n = 3)	4.60 ± 0.20	3.3 ± 0.10	3.7 ± 0.10
Double-Layer Capacitance, Cdl (mF, n = 3)	4.51 ± 0.03	0.681 ± 0.010	0.376 ± 0.005
Constant Phase Element, CPE (mMho, n = 3)	47.4 ± 0.3	92.4 ± 0.4	81.1 ± 0.3

Table 4. Comparison of Electrochemical Performance Parameters of Pristine TCWAC and Its MnO_2- and Fe_2O_3-Modified Composite. Parameters Include Potential Window, Specific Capacitance, Energy Density, Power Density, Capacity Retention, and Equivalent Series Resistance (ESR) Each Reported as Mean ± Standard Deviation (n = 3).

Electrodes	Potential Windows(V)	Specific Capacitance (Fg^{-1} at 1 Ag^{-1}, n = 3)	Energy Density ($Whkg^{-1}$, n = 3)	Power Density ($Whkg^{-1}$, n = 3)	Capacity retention (% after 1000 cycles, n = 3)	ESR (Ω, n=3)
TCWAC	−1.0 to −0.2	156.3 ± 1.08	3.5 ± 0.17	371.4 ± 5.38	80.2 ± 0.66	0.43 ± 0.017
TCWAC-Mn	−1.2 V to 0	489.4 ± 6.36	25.1 ± 0.72	376.1 ± 4.89	99.1 ± 0.29	0.38 ± 0.017
TCWAC-Fe	−1.15 to −0.4	321.3 ± 2.80	6.3 ± 0.26	296.2 ± 1.57	90.3 ± 0.62	0.41 ± 0.020

3. Results and Discussion

3.1. Physicochemical Characterization of TCWAC: Establishing Structure–Performance Relationship

To assess the potential of *Toona ciliata* wood scrap-derived activated carbon (TCWAC) as a sustainable electrode material for energy storage, we employed a comprehensive suite of physicochemical characterization techniques. This included X-ray diffraction (XRD), Raman spectroscopy, scanning and transmission electron microscopy (SEM and TEM), Brunauer–Emmett–Teller (BET) surface area analysis, Fourier-transform infrared spectroscopy (FTIR), and X-ray photoelectron spectroscopy (XPS). Each technique was selected to elucidate a key structural or surface feature that governs electrochemical performance in supercapacitor systems:

- **XRD** assessed crystallinity and the presence of amorphous carbon domains, which are critical for

charge storage efficiency.

- **Raman spectroscopy** evaluated graphitization (G-band) and structural disorder (D-band), offering insight into conductive pathways and defect density.
- **BET analysis** measured specific surface area and pore size distribution, which govern ion accessibility and double-layer formation.
- **SEM and TEM** visualized porous architecture and morphological uniformity at micro- and nanoscale levels, correlating with ion diffusion.
- **FTIR spectroscopy** identified surface functional groups—particularly oxygen-containing moieties—that can enhance pseudocapacitive behavior and improve wettability.
- **XPS** revealed elemental composition and chemical states on the carbon surface, providing evidence of heteroatom doping or residual oxygen functionalities.

Together, these results demonstrate that TCWAC features a desirable combination of high surface area, well-developed porosity, appropriate surface chemistry, and controlled structural disorder. These attributes work synergistically to deliver efficient electrochemical performance. The findings confirm that this bio-derived carbon, produced via a low-temperature, phosphoric acid-assisted activation serves as a viable and sustainable electrode material for supercapacitor applications.

3.2. Structural Disorder and Amorphous Nature of TCWAC: Insights from XRD and Raman Spectroscopy

The electrochemical performance of carbon-based materials strongly depends on their structural order, graphitization level, and defect density. To examine these features in TCWAC, we used X-ray diffraction (XRD) and Raman spectroscopy were employed—two complementary techniques that reveal key information about crystallinity and structural disorder (**Figure 1**).

3.2.1. XRD Analysis

The XRD pattern shows a broad diffraction peak centered around 2θ ≈ 26°, corresponding to the (002) plane of graphitic carbon (**Figure 1(a)**). The low intensity and diffuse nature of this peak confirms a largely amorphous carbon structure characterized by turbostratic stacking and minimal long-range order. A weaker peak near 2θ ≈ 43°, attributed to the (100) plane, suggests indicates the presence of minor graphitic microdomains within the disordered matrix.

This configuration—predominantly amorphous with localized graphitic clusters—strikes a balance ideal for supercapacitor applications. The amorphous regions enhance ion accessibility and surface reactivity, while the sparse graphitic domains contribute electrical conductivity and charge transport [11].

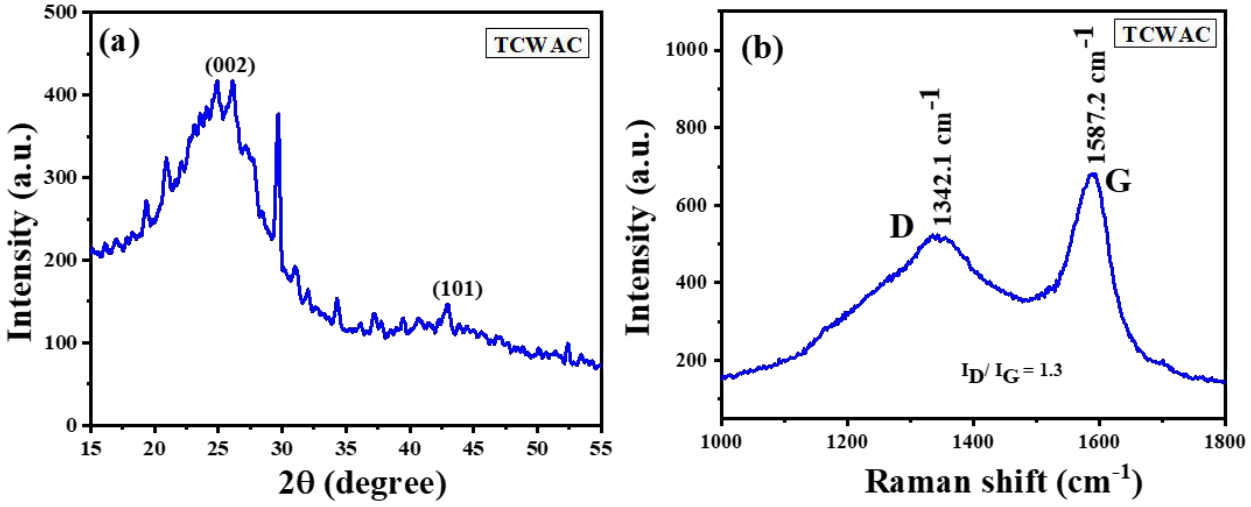

Figure 1. (a) XRD Pattern of TCWAC Showing a Broad (002) Peak and Minor (100) Reflection, Confirming Its Largely Amorphous Nature. **(b)** Raman Spectrum of TCWAC Showing D and G Bands with ID/IG ≈ 1.3, Indicating High Structural Disorder.

3.2.2. Raman Spectroscopy

Raman analysis supports the XRD findings (**Figure 1(b)**). Two prominent bands appear: the D-band (~1350 cm^{-1}), associated with structural defects and disordered carbon atoms, and the G-band (~1580 cm^{-1}), reflecting the presence of sp^2-bonded graphitic carbon. The intensity ratio (ID/IG ≈ 1.3) suggests a high degree of disorder consistent with an amorphous framework.

Such structural disorder is advantageous, generating abundant electrochemically active sites and enabling rapid ion adsorption. Partial graphitization sufficient electronic conductivity, creating a synergistic structure well-suited for fast charge–discharge cycles in supercapacitor systems.

3.2.3. Sustainability Perspective

The ability to engineer this desirable structure using low-temperature acid-assisted activation—without high-temperature graphitization—demonstrates the sustainability of TCWAC. Derived from locally available biomass waste and processed via eco-compatible methods, TCWAC offers a low-cost, energy-efficient pathway route to high-performance carbon electrodes.

3.3. Morphological and Textural Properties of TCWAC: SEM, TEM, and BET Insights

The morphology and porosity of carbon materials critically influence their electrochemical behavior. For TCWAC, we examined surface architecture and textural properties using scanning electron microscopy (SEM), transmission electron microscopy (TEM), and Brunauer–Emmett–Teller (BET) surface area analysis. These techniques provide insights into ion transport, electrolyte accessibility, and charge storage capacity—key parameters that determine electrode performance in supercapacitors.

3.3.1. Surface Morphology: SEM Analysis

The SEM micrograph (**Figure 2**) displays a highly porous surface with irregular, interconnected pores distributed across a rough carbon matrix. This unique morphology results from phosphoric acid (H_3PO_4) activation, where chemical etching during carbonization creates abundant voids and channels.

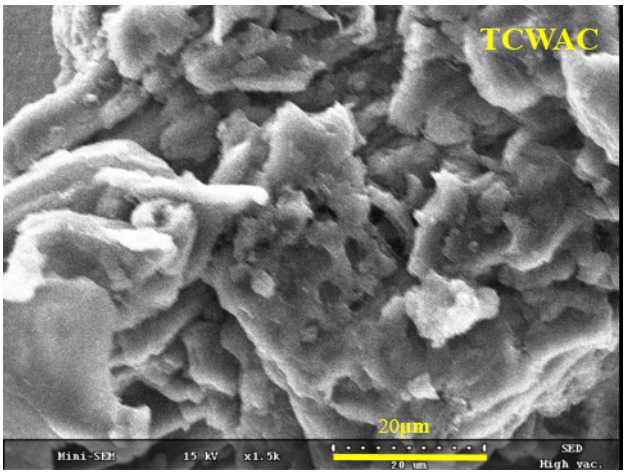

Figure 2. SEM Image of TCWAC Showing Irregular, Interconnected Pores with a Rough Surface (Scale Bar = 20 µm).

Such a porous network facilitates electrolyte ions infiltration, reduces diffusion distances, and promotes efficient ion exchange at the electrode–electrolyte interface. The presence of surface defects and structural irregularities further supports the amorphous carbon structure identified through XRD and Raman spectroscopy. Although these features reduce graphitic order, they significantly increase the number of accessible electroactive sites, thereby enhancing capacitive behavior [11].

3.3.2. Textural Properties: BET Surface Area and Pore Size Distribution

The nitrogen adsorption–desorption isotherm of TCWAC (**Figure 3**) exhibits a distinct Type IV hysteresis loop, a hallmark of mesoporous structures. BET analysis yielded a high specific surface area of **1453** ± 29 $\mathbf{m^2g^{-1}}$, an average pore diameter of **4.1** ± 0.2 **nm**, and a total pore volume of **1.5** ± 0.1 $\mathbf{cm^3g^{-1}}$, each reported as mean ± standard deviation (n = 3).

Since the composite preparation involved physical mixing without high-temperature treatment, no significant changes in surface area or pore structure are expected in TCWAC–Mn and TCWAC–Fe composites. Their electrochemical enhancements are therefore attributed primarily to pseudocapacitive contributions of the introduced metal oxides, rather than further textural modifications.

This mesopore-rich structure offers several advantages

for supercapacitor applications. The extensive surface area ensures a large number of active sites for charge storage, while the interconnected mesoporous channels promote rapid electrolyte transport and reduce ion diffusion resistance. These attributes collectively support efficient double-layer formation high-rate charge–discharge cycling [12,13].

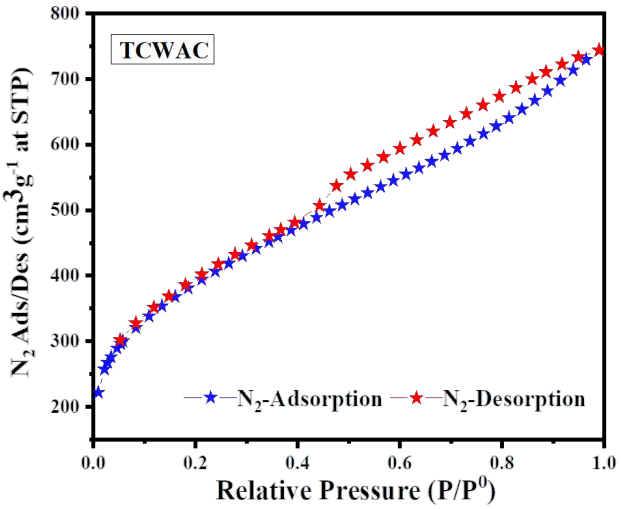

Figure 3. N_2 Adsorption–Desorption Isotherm of TCWAC Showing Type IV Behavior with a Pronounced Hysteresis Loop, Confirming Mesoporosity.

3.3.3. Internal Structure: TEM Observations

TEM analysis (**Figure 4**) reveals a disordered amorphous carbon matrix interspersed with randomly oriented mesopores. The absence of crystalline lattice fringes confirms the non-graphitic turbostratic structure of TCWAC, aligning with previous structural analyses [14–17].

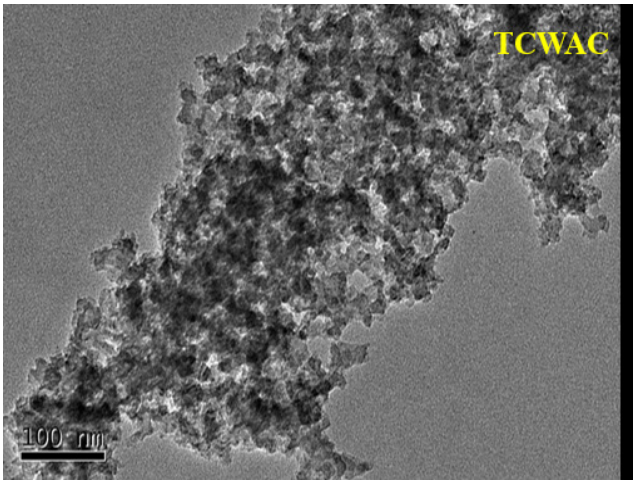

Figure 4. TEM Image of TCWAC Showing Nanoscale Porosity Within an Amorphous Carbon Framework (Scale Bar = 100 nm).

The heterogeneous pore distribution and nanoscale domain architecture promote fast ion transport, enhance charge transfer kinetics, and improve ionic conductivity throughout the electrode matrix.

Collective Impact:

The synergy of high surface area, mesoporosity, interconnected pore networks, and internal disorder creates a structurally optimized platform for efficient charge storage. These attributes collectively account for the superior electrochemical performance of TCWAC as a sustainable electrode material for supercapacitor applications [18,19].

3.3.4. Surface Chemistry and Functional Group Analysis

1. Functional Group Identification via FTIR and Correlation with XPS

The surface chemistry of TCWAC was systematically characterized using Fourier-transform infrared spectroscopy (FTIR) and X-ray photoelectron spectroscopy (XPS) to identify functional groups and chemical environments critical for electrolyte wettability, redox activity, and ion accessibility—key parameters for high-performance supercapacitors.

The FTIR spectrum (**Figure 5**) shows a broad band around **~3400 cm⁻¹**, corresponding to O–H stretching vibrations from hydroxyl groups, possibly arising from phenolic structures or adsorbed moisture. XPS O 1s analysis (**Figure 6**) reveals a peak at **~532.2 eV,** confirming C–O bonding environments such as hydroxyls and ethers and highlighting the oxygen-rich surface [20,21].

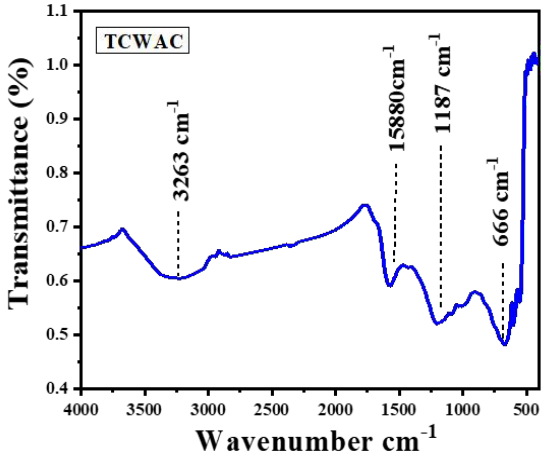

Figure 5. FTIR Spectrum of TCWAC Indicating–OH, C=O, C–O, and Aromatic C=C Groups.

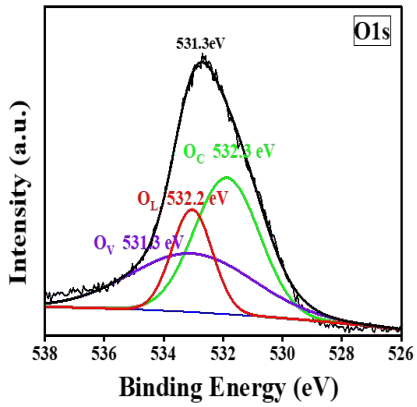

Figure 6. XPS Analysis of TCWAC: O 1s Peaks (C=O: ~531.3 eV, C–O: ~532.2 eV).

A distinct FTIR peak near **~1700 cm⁻¹** corresponds to C=O stretching from carbonyl and carboxylic acid groups. This is corroborated by the deconvoluted XPS C 1s peak at **~288.0 eV,** the O 1s signal at **~531.3 eV** (**Figure 7**), both indicative of oxygenated carbon species [22,23].

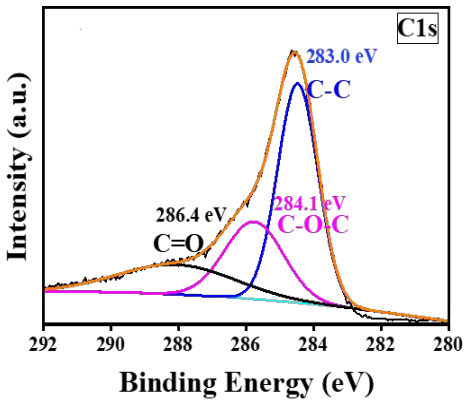

Figure 7. XPS Analysis of TCWAC: High-Resolution C 1s Spectrum (C–C: ~284.6 eV, C–O: ~286.4 eV, C=O: ~288.0 eV).

The FTIR band around **~1600 cm⁻¹** is attributed to aromatic C=C stretching, reflecting sp^2-hybridized carbon domains. This aligns with the dominant C 1s peak at ~ **284.6 eV** in the XPS spectrum, which denotes graphitic or partially disordered aromatic structures.

Additional FTIR features in the **1200–1000 cm⁻¹** region represents C–O stretching vibrations from alcohols, ethers, or esters. Corresponding XPS peaks at **~286.4 eV (C 1s)** and **~532.2 eV (O 1s),** further confirm the incorporation of oxygen-containing functionalities during H_3PO_4 activation.

Notably, the XPS survey spectrum (**Figure 8**) also reveals a distinct **P 2p peak at ~133 eV**, indicating successful phosphorus incorporation into the carbon matrix—undetectable by FTIR due to elemental limitations. Phosphorus enhances surface acidity and hydrophilicity, thereby promoting improved electrolyte wettability and ion transport [24,25].

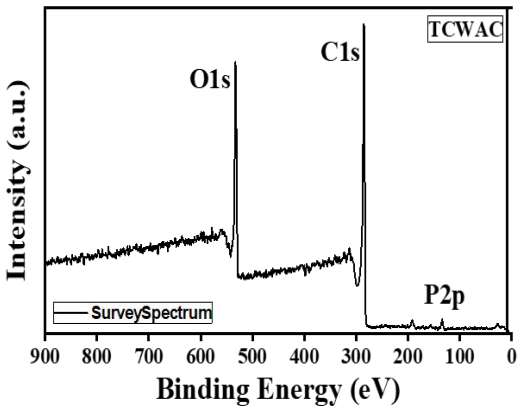

Figure 8. XPS Analysis of TCWAC: Survey Spectrum Showing C, O, and P Signals.

Integrated Structural Advantages:

The combined results from XRD, Raman, SEM, TEM, BET, FTIR, and XPS—collectively reveals a material with characteristics highly favorable for electrochemical energy storage:

- **Highly porous morphology:** SEM and BET analyses confirm an interconnected pore network that facilitates efficient electrolyte diffusion and ion transport [26].
- **Optimized mesoporosity:** The mesoporous architecture enhances double-layer formation and charge transport kinetics [27].
- **Amorphous carbon framework:** XRD and Raman data reveal a disordered matrix that increases active surface sites and capacitance [28].
- **Oxygen-rich surface chemistry:** FTIR and XPS show abundant oxygen-containing groups that improve wettability and pseudocapacitive behavior [29].

These synergistic characteristics confirm that H_3PO_4 activation effectively converts biomass waste into a structurally and chemically optimized carbon material, well-suited for energy storage.

Building on this robust structural and chemical foundation, the next section examines the electrochemical performance of TCWAC and its composites (TCWAC-Mn and TCWAC-Fe), highlighting their practical suitability for high-performance supercapacitor applications.

3.5. Electrochemical Characterization of TCWAC Electrode and Its Composites

3.5.1. Cyclic Voltammetry (CV)

Cyclic voltammetry was conducted to evaluate the charge storage mechanism and capacitive behavior of the TCWAC electrode, as well as its composites with MnO_2 and Fe_2O_3.

As shown in **Figure 9**, the TCWAC electrode exhibits nearly rectangular CV profile across all scan rates a hallmark of ideal electric double-layer capacitance (EDLC). The absence of redox peaks confirms a non-faradaic charge storage mechanism typical of porous derived from biomass. Notably, the CV shape remains consistent even at a high scan rate of 100 mVs^{-1}, reflecting efficient ion diffusion, minimal internal resistance, and excellent electrochemical reversibility. The high current response (~12 Ag^{-1}) further demonstrates the electrode's capacitive efficiency, affirming TCWAC as a promising EDLC electrode material [30].

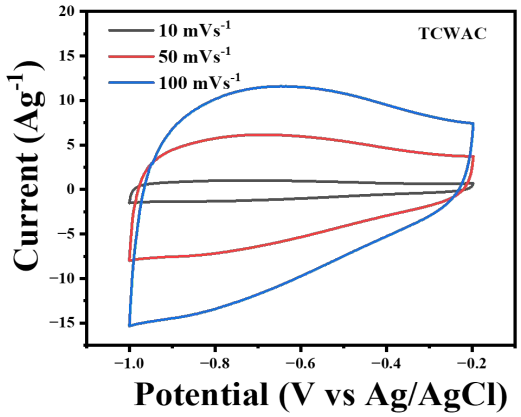

Figure 9. CV Curves of TCWAC Electrode at Varying Scan Rates (Potential Window: −1.0 to −0.2 V).

3.5.2. Composite Electrodes and Performance Enhancement

To improve overall electrochemical performance, TCWAC was composited with MnO_2 and Fe_2O_3 in a 1:1 weight ratio, and CV analyses were performed within tailored potential windows.

In **Figure 10**, the TCWAC-Mn electrode exhibits prominent redox peaks over −1.2 to 0 V, indicative of pseudocapacitive behavior introduced by MnO_2. This broad potential window (−1.2 to 0 V) enables MnO_2 to fully access its redox transitions (Mn^{4+}/Mn^{3+} and Mn^{3+}/Mn^{2+}), enhancing ion accessibility and accelerating charge transfer processes. This synergistic interaction between TCWAC's high surface area and MnO_2's redox activity significantly improves capacitive performance [7,31].

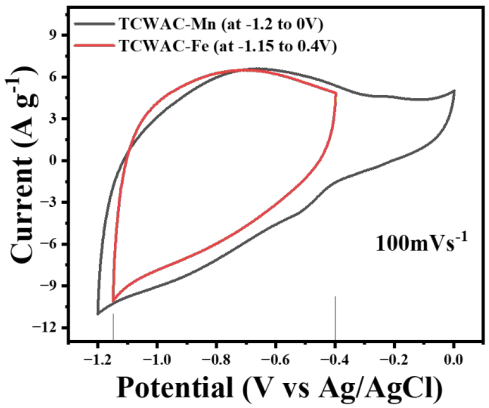

Figure 10. CV Curves of TCWAC-Mn and TCWAC-Fe Electrodes at 100 mVs^{-1}. Potential Windows: −1.2 to 0 V (TCWAC-Mn) and −1.15 to −0.4 V (TCWAC-Fe).

Conversely, applying the same wide potential window to the TCWAC-Fe electrode resulted in diminished performance. This is likely due to Fe_2O_3's narrower electrochemical stability range and sluggish redox kinetics, which caused instability. Upon reducing the window to −1.15 to −0.4 V—better aligned with Fe_2O_3's redox potential—the composite displayed more stable CV behavior and improved reversibility [2,3,32].

Key Insight:

These findings underscore the importance of potential window optimization in composite electrodes. MnO_2 enables robust pseudocapacitive performance over a wide voltage range. Fe_2O_3 requires a narrower and more selective window to maintain electrochemical stability and reproducibility. This tailored approach ensures each material operates under conditions that maximize its intrinsic electrochemical properties.

3.6. Galvanostatic Charge-Discharge (GCD) Analysis

Galvanostatic charge-discharge (GCD) measurements were carried out to complement cyclic voltammetry (CV)

data and provide further insight into the charge storage performance of the TCWAC electrode and its composites. As with CV, selection of an appropriate potential window—particularly for redox-active materials— is critical for extracting meaningful and reproducible electrochemical data [10].

3.6.1. TCWAC Electrode

The GCD profile of the pristine TCWAC electrode (**Figure 11**), recorded within the −1.0 to −0.2 V-range. exhibits a nearly symmetric triangular shape, characteristic of ideal electric double-layer capacitance (EDLC). The uniform charge–discharge behavior reflects high coulombic efficiency, good reversibility, and minimal internal resistance. A discharge time of approximately 110 s was observed at a current density of 1 Ag^{-1}, indicating favorable capacitive characteristics.

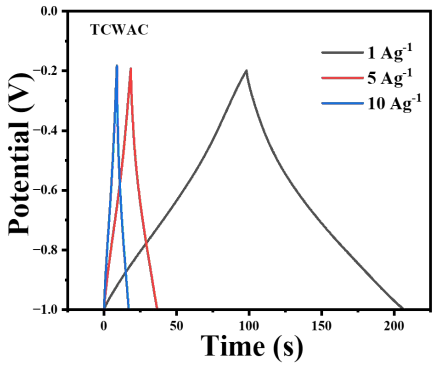

Figure 11. GCD Curve of TCWAC Electrode at 1 Ag^{-1} in the Potential Window of −1.0 to −0.2 V.

The specific capacitance (Cs) was calculated using the standard formula:

$$Cs = \frac{I\Delta t}{m\Delta V} \quad (1)$$

Where:

- Cs is the specific capacitance (Fg^{-1})
- I is the discharge current (A)
- Δt is the discharge time (s)
- m is the mass of active material (g)
- ΔV is the potential window (V)

3.6.2. Composite Electrodes

(1) TCWAC-Mn Composite

The TCWAC-Mn electrode exhibits a distinct non-linear GCD profile, indicative of combined EDLC and pseudocapacitive behavior due to MnO_2. Measurement within a broadened potential window of −1.2 to 0 V enabled full utilization of MnO_2's redox activity (**Figure 12**) [33]. A notably long discharge time of ~600 s was observed at 1 Ag^{-1}, corresponding to a high specific capacitance of 489.4 Fg^{-1}. This performance highlights the synergistic contribution of TCWAC's porous structure and MnO_2's faradaic redox processes, leading to enhanced charge storage capacity.

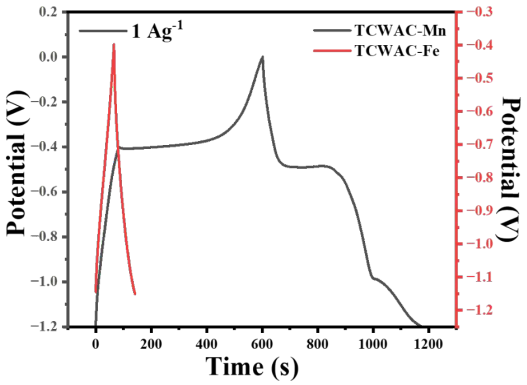

Figure 12. GCD Curves of TCWAC-Mn and TCWAC-Fe Electrodes at 1 Ag^{-1}; Potential Windows: –1.2 to 0 V (TCWAC-Mn), –1.15 to –0.4 V (TCWAC-Fe).

(2) TCWAC-Fe Composite

For the TCWAC-Fe composite, GCD testing was conducted within a narrower window (−1.15 to −0.4 V), due to the limited redox activity and stability of Fe_2O_3 outside this range. The resulting GCD curve retained a mostly triangular shape with slight deviations, suggesting predominant EDLC behavior with modest faradaic contribution (**Figure 12**). A discharge time of ~100 s was recorded at 1 Ag^{-1}, yielding a specific capacitance of 321.3 Fg^{-1}. Although this is significantly higher than that of the pristine TCWAC electrode, it remains lower than the MnO_2 composite, reflecting the relatively subdued pseudocapacitive effect of Fe_2O_3 [34–36].

The comparatively lower electrochemical performance of the TCWAC-Fe composite may be attributed to several interrelated factors. The cyclic voltammetry profiles (**Figure 10**) reveal largely EDLC-like behavior with only minor faradaic contributions, suggesting limited reversibility of Fe^{3+}/Fe^{2+} redox transitions within the applied potential window. This is further corroborated by electrochemical impedance spectroscopy results (**Table 3**), where

the TCWAC-Fe electrode exhibits a higher charge transfer resistance (Rct = 0.143 Ω) compared to TCWAC-Mn (Rct = 0.110 Ω), reflecting slower interfacial electron transfer kinetics and reduced charge transfer efficiency. The intrinsic lower electrical conductivity of Fe_2O_3, combined with its less reversible redox reactions, results in sluggish redox kinetics, thereby limiting pseudocapacitive contribution under dynamic cycling conditions.

Additionally, Fe_2O_3 is known to undergo partial dissolution or structural degradation in alkaline electrolytes during extended cycling, which can progressively diminish active redox sites and compromise capacitance retention [37,38]. Although the TCWAC-Fe electrode demonstrated reasonably good stability over 1000 cycles, such degradation pathways may still contribute to performance limitations, especially under prolonged high-rate operation. These combined factors account for the relatively subdued capacitive performance of the Fe_2O_3 composite.

Collectively, these GCD results validate that integrating MnO_2 with TCWAC significantly boosts pseudocapacitive performance, whereas Fe_2O_3 offers moderate enhancement under optimized electrochemical conditions.

(3) Comparative Insight

These GCD findings reinforce the earlier CV results, clearly demonstrating that:

- **MnO_2 integration** significantly enhances capacitance through efficient redox reactions and extended operating potential.
- **Fe_2O_3 integration** provides moderate improvements under a narrower voltage range, primarily governed by EDLC behavior with minor pseudocapacitive support.

Thus, **MnO_2 proves more effective than Fe_2O_3** in augmenting the electrochemical performance of TCWAC-based electrodes under the evaluated conditions.

3.7. Specific Capacitance Across Electrodes

The variation in specific capacitance of TCWAC and its composite electrodes with increasing current density was analyzed using Equation (1). The results are summarized in **Table 1**. These trends provide valuable insight into the rate capability and electrochemical efficiency of each electrode system.

Figure 13 presents the variation of specific capacitance as a function of current density for TCWAC, TCWAC-Mn, and TCWAC-Fe electrodes, clearly illustrating the trends summarized in **Table 1**.

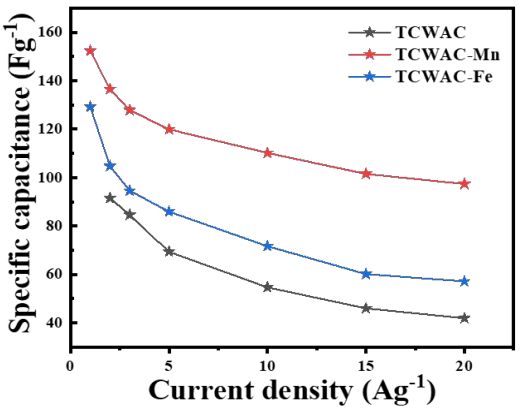

Figure 13. Specific Capacitance of TCWAC-Electrode, TCWAC-Mn and TCWAC-Fe Electrodes as a Function of Current Density.

The pristine **TCWAC electrode** exhibited a characteristic decline in specific capacitance with increasing current density, a typical behavior of electric double-layer capacitors (EDLCs). The capacitance decreased from 156.3 ± 1.08 Fg^{-1} at 1 Ag^{-1} to 33.3 ± 0.9 Fg^{-1} at 20 Ag^{-1}, primarily due to the restricted diffusion of electrolyte ions at higher charge–discharge rates. At elevated current densities, only the outer surface of the electrode is effectively accessed by ions, resulting in reduced utilization of the internal porous network.

In contrast, the **TCWAC-Mn composite** displayed substantially higher specific capacitance and excellent retention across all current densities. Starting at 489.4 ± 6.36 Fg^{-1} at 1 Ag^{-1}, the capacitance remained as high as 97.4 ± 2.0 Fg^{-1} at 20 Ag^{-1}, retaining nearly 20% of its initial capacity even at rapid discharge rates. This superior rate capability is attributed to the pseudocapacitive contribution of MnO_2, which undergoes fast and reversible redox reactions. Moreover, the stabilization of capacitance values beyond 10 Ag^{-1} suggests robust ion transport kinetics and structural integrity under dynamic operating conditions [39,40].

The TCWAC-Fe composite also exhibited improved performance over the pristine TCWAC, achieving 321.3 ± 2.80 Fg^{-1} at 1 Ag^{-1}. However, its overall capacitance values were lower than those of the MnO_2-based composite, decreasing more sharply with increasing current. At 20 Ag^{-1}, it reached only 33.6 ± 0.8 Fg^{-1}, nearly equivalent to that of TCWAC. This performance decline is likely due to

Fe_2O_3's lower electrical conductivity and limited redox reversibility, which constrain charge transfer and ion mobility during high-rate cycling.

These results clearly highlight the electrochemical superiority of the TCWAC-Mn composite, particularly at elevated current densities. Its outstanding capacitance retention and high-rate performance are indicative of a hybrid charge storage mechanism**,** where the porous carbon matrix facilitates EDLC**,** and MnO_2 introduces pseudocapacitive redox reactions**.** This dual functionality makes TCWAC-Mn a highly promising electrode material for next-generation high-performance supercapacitors. The high retention of capacitance at elevated current densities also reflects the efficient coupling between MnO_2's pseudocapacitance and the fast ion transport enabled by the hierarchical porosity of TCWAC.

3.8. Power and Energy Density Evaluation

To assess the practical applicability of the TCWAC-based electrodes in energy storage devices, their **energy density (ED)** and **power density (PD)** were calculated from GCD profiles using the following equations:

$$ED = Cs \times V \times \frac{\Delta t}{8} \times 3.6 \quad (2)$$

$$PD = \frac{ED}{\Delta t} \quad (3)$$

Where:

- Cs is the specific capacitance (Fg^{-1})
- V is the operating potential window (V),
- Δt is the discharge time (s),
- ED is the energy density ($Whkg^{-1}$)
- PD is the power density (Wkg^{-1})

The factor of 8 in Equation (2) accounts for the three-electrode configuration (i.e.,only the working electrode is considered), and the constant 3.6 converts joules per gram ($J\ g^{-1}$) to watt-hours per kilogram ($Wh\ kg^{-1}$) [7,8,40–42].

3.8.1. Ragone Plot Analysis

The Ragone plot (energy density vs. power density) presented in **Figure 14** illustrates the comparative energy–power performance of the TCWAC, TCWAC–Mn, and TCWAC–Fe electrodes.

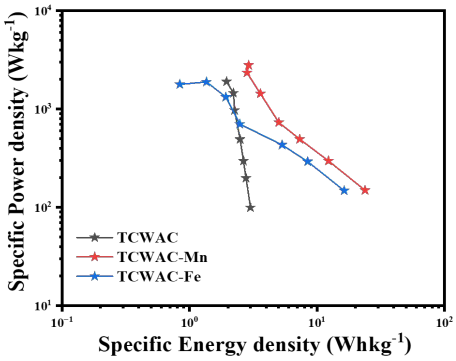

Figure 14. Ragone Plots of TCWAC, TCWAC–Mn, and TCWAC–Fe Electrodes.

3.8.2. Performance Insights

TCWAC–Mn Composite:

- Achieved the highest energy density (**25.1 Wh kg^{-1}**) and power density (**371.4 W kg^{-1}**), significantly outperforming both pristine TCWAC and the Fe_2O_3-based composite.
- This enhanced performance is attributed to the **synergistic integration of MnO_2**, which provides both electric double-layer capacitance and faradaic (pseudocapacitive) contributions.

3.8.3. Mechanistic Insights

MnO_2-based electrode (TCWAC–Mn):

- Operates through **fast and** via reversible **Mn^{4+}/Mn^{3+}** redox transitions, enhancing charge storage.
- Efficient **K^+ ion intercalation**, ensuring rapid charge transport and minimizing resistance.
- Delivers a **hybrid capacitance behavior**, effectively combining EDLC and **pseudocapacitance** mechanisms, resulting in both high energy storage and rate capability [43–46].

Fe_2O_3-based electrode (TCWAC–Fe):

- Relies on **Fe^{3+}/Fe^{2+}** redox transitions, but exhibits **limited reversibility and lower electrical conductivity.**
- Constrained by a **narrower potential window**, and **slower redox kinetics**, which limit energy and power output compared to MnO_2-based composites [37,38].

3.8.4. Comparative Summary

The TCWAC–Mn electrode stands out as the most

promising candidate, benefiting from:

- **Higher redox activity** and **reversibility**
- **Broader electrochemical window** (–1.2 to 0 V)
- **Superior ion transport** within the porous carbon–MnO_2 hybrid matrix

These characteristics enable **high energy density with excellent power performance**, positioning MnO_2-integrated carbon electrodes as a compelling material system for next-generation **high-rate, high-capacity supercapacitors** [47–49]. These Ragone plot results strongly suggest that the combination of high mesoporosity and accessible surface functionality in TCWAC-Mn enables efficient electrolyte penetration and ion diffusion, which, together with MnO_2's reversible redox transitions, leads to improved energy and power delivery over a wide operating window.

3.9. Electrochemical Impedance Spectroscopy (EIS) Analysis

Electrochemical impedance spectroscopy (EIS) provided valuable insights into the resistive and capacitive properties of the TCWAC, TCWAC–Mn, and TCWAC–Fe electrodes. Nyquist plots (**Figure 15**), recorded in 6 M KOH electrolyte over the frequency range of 100 kHz to 0.1 Hz using a 10 mV AC perturbation, revealed key parameters related to charge transfer resistance, ion diffusion, and double-layer behavior of the electrodes [45,50].

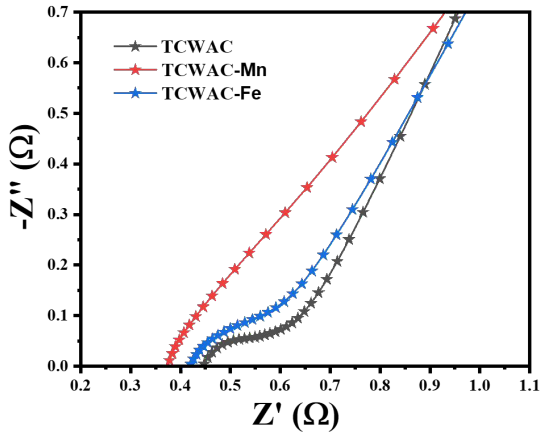

Figure 15. Nyquist Plots of TCWAC, TCWAC–Mn, and TCWAC–Fe Electrodes in 6M KOH.

Table 3 summarizes the extracted EIS-derived parameters—solution resistance (Rs), charge transfer resistance (Rct), Warburg impedance (W), specific capacitance (Cs), double-layer capacitance (Cdl), and the constant phase element (CPE)— presented as mean ± standard deviation (n = 3).

Interpretation:

Among the three electrodes, the TCWAC–Mn composite exhibited the lowest Rs (0.38 Ω), Rct (0.11 Ω), and Warburg impedance (3.3 Ω), clearly indicating superior electrical conductivity, faster charge transfer kinetics, and enhanced ion diffusion. By comparison, TCWAC–Fe and TCWAC showed higher Rct values (0.143 Ω and 0.173 Ω, respectively), confirming that MnO_2 incorporation more effectively promotes electron mobility.

The lower Warburg impedance of TCWAC–Mn further highlights its improved ion transport characteristics—critical for sustaining high performance during rapid charge/discharge cycles. Its higher CPE value (92.4 mMho) reflects stronger pseudocapacitive behavior and greater surface heterogeneity, both of which contribute to enhanced energy storage capacity.

These improvements are attributed to:

- **Reversible** Mn^{4+}/Mn^{3+} redox transitions in MnO_2.
- **Better integration** of MnO_2 into the porous TCWAC matrix, facilitating fast ion diffusion.
- **Synergistic interactions** between MnO_2 and the conductive carbon framework, which enable efficient electron and ion transport [37,44,49,51–53].

The integration of MnO_2 into the highly porous TCWAC framework reduces charge transfer resistance and enhances diffusion pathways due to strong interfacial contact. This synergistic interface facilitates faster electron hopping and ion migration, which directly supports high-rate capability and long-term electrochemical stability observed in TCWAC–Mn composites.

Equivalent Circuit Model

To quantify the EIS data, the Nyquist plots were fitted using an equivalent circuit model (**Figure 16**), consisting of Rs, Rct, Cdl, W, and CPE components. This model accurately represented the frequency-dependent electrochemical behavior of all electrodes, yielding a strong correlation across the entire spectrum.

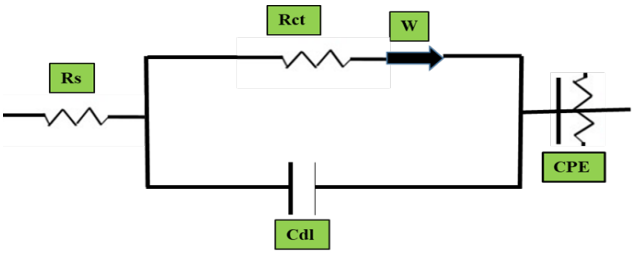

Figure 16. Equivalent Circuit Model Used to Fit the EIS Data for TCWAC, TCWAC–Mn, and TCWAC–Fe Electrodes.

3.10. Capacity Retention Analysis

Cycling stability is a crucial factor in determining the long-term performance of supercapacitor electrodes. To evaluate this, the TCWAC, TCWAC–Mn, and TCWAC–Fe electrodes were subjected to 1000 continuous charge–discharge cycles at a current density of 3 Ag^{-1} (**Figure 17**).

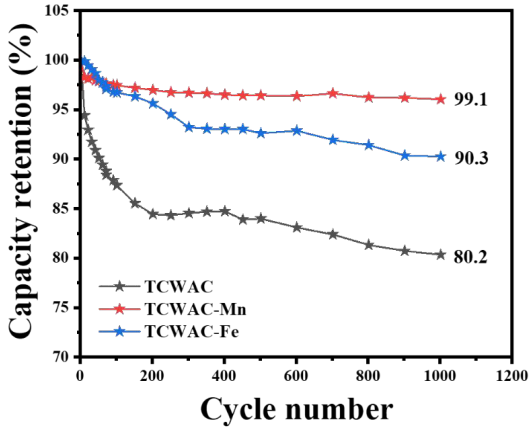

Figure 17. Capacity Retention Profiles of TCWAC, TCWAC–Mn, and TCWAC–Fe Electrodes Over 1000 Charge–Discharge Cycles at 3 Ag^{-1}. The TCWAC–Mn Composite Demonstrates Remarkable Retention of 99.1%.

The pristine TCWAC electrode retained **80.2%** of its initial specific capacitance, indicating moderate durability. The TCWAC–Fe composite demonstrated improved performance, maintaining **90.3%** of its original capacitance—suggesting better structural integrity and electrochemical resilience. Most notably, the TCWAC–Mn composite exhibited **exceptional stability**, retaining **99.1%** of its initial capacitance after 1000 cycles. This superior retention highlights its outstanding long-term electrochemical reliability [3,4,53–55].

Mechanistic Factors Underpinning the Superior Performance of TCWAC–Mn

- MnO_2 offers multiple accessible oxidation states **($Mn^{4+}/Mn^{3+}/Mn^{2+}$),** enabling highly reversible faradaic redox reactions that enhance pseudocapacitance.
- Lower charge transfer resistance (Rct), as confirmed by EIS, supports faster charge-transfer kinetics at the electrode–electrolyte interface.
- The hierarchical porous architecture of TCWAC facilitates efficient ion diffusion and electrolyte accessibility, ensuring stable charge storage even under prolonged cycling.
- The robust carbon–MnO_2 network architecture withstands volumetric changes during redox cycling without structural degradation.

In contrast, Fe_2O_3 provides redox-driven charge storage via Fe^{3+}/Fe^{2+} transitions but suffers from lower electrical conductivity and slower charge transfer kinetics, which limits its cycling durability and capacitance retention.

While excellent stability was demonstrated over 1000 cycles, it is acknowledged that for practical industrial applications, extended long-term cycling evaluations (typically exceeding 5000–10,000 cycles) are commonly required to fully establish durability under operational conditions. Due to laboratory time constraints and equipment limitations, such extended cycling could not be performed in this study but will be pursued in future investigations to further validate the electrode's practical scalability.

4. Conclusions

This study demonstrates a simple and scalable pathway for converting renewable *Toona ciliata* wood scrap—a locally abundant and underutilized biomass—into high-performance activated carbon (TCWAC) for supercapacitor applications through single-step carbonization and phosphoric acid activation. The resulting TCWAC exhibited high surface area, well-developed hierarchical porosity, and favorable electrical conductivity.

Integration of transition metal oxides (MnO_2 and Fe_2O_3) with TCWAC significantly enhanced the electrochemical performance. Among the composites, TCWAC–Mn delivered the best results, achieving a high specific capacitance of **489.4 Fg^{-1}** at 1 Ag^{-1}, an energy density of **25.1 $Whkg^{-1}$**, and excellent cycling stability with **99.1%** capacitance retention after 1000 cycles. The superior performance of MnO_2 is attributed to its multiple acces-

sible oxidation states enabling reversible redox reactions, improved charge transfer kinetics (as indicated by EIS analysis), and efficient ion diffusion through the porous carbon network. In contrast, while TCWAC–Fe exhibited improved performance over pristine TCWAC, its lower electrical conductivity and slower redox kinetics resulted in comparatively reduced capacitive behavior.

The Fe_2O_3-based composite (TCWAC–Fe) also outperformed the pristine TCWAC, achieving a specific capacitance of **321.3 Fg^{-1}** and energy density of **6.3 $Whkg^{-1}$**. However, its lower electrical conductivity and sluggish redox kinetics limited its performance compared to MnO_2-integrated electrode (TCWAC–Mn). **Table 4** provides a comparative overview of the electrochemical characteristics of pristine and composite electrode materials.

This work provides a direct comparative evaluation of MnO_2 and Fe_2O_3 composites on an identical biomass-derived carbon matrix under fully standardized synthesis and testing conditions, offering valuable mechanistic insight into their distinct charge storage behaviors—an approach rarely explored in biomass-carbon supercapacitor literature.

While these findings demonstrate promising laboratory-scale performance, further research is necessary to advance practical applicability. Future studies should focus on optimizing composite formulations, investigating greener synthesis routes, conducting extended long-term cycling (>10,000 cycles), scaling up synthesis processes, performing full device assembly, and incorporating techno-economic analysis to evaluate commercial feasibility.

Mechanistically, the superior performance of TCWAC–Mn is attributed to the optimized interface between redox-active MnO_2 particles and the mesoporous carbon matrix, which enhances charge transfer kinetics, redox reversibility, and ion accessibility—key factors for advanced supercapacitor applications.

Mechanistically, the superior performance of TCWAC–Mn is attributed to the optimized interface between redox-active MnO_2 particles and the mesoporous carbon matrix, which enhances charge transfer kinetics, redox reversibility, and ion accessibility—key factors for advanced supercapacitor applications.

Overall, this work contributes to sustainable material development by converting locally available wood waste into functional energy storage materials, supporting resource-efficient utilization of biomass while reducing environmental burden.

Funding

This work received no external funding.

Institutional Review Board Statement

Not applicable.

Informed Consent Statement

Not applicable.

Data Availability Statement

The data supporting the findings of this study are available from the corresponding author upon reasonable request.

Acknowledgments

The author expresses sincere gratitude to the Central Department of Chemistry, Tribhuvan University, Kirtipur, Nepal, and Patan Multiple Campus, Institute of Science and Technology, Tribhuvan University, Patan Dhoka, Lalitpur, Nepal, for providing the essential laboratory facilities required to conduct this research. Special appreciation is extended to the Global Research Laboratory (GRL) at Sun Moon University, South Korea, and the Advanced Functional Material Physics (AMP) Laboratory at Suranaree University of Technology (SUT), Thailand, for their invaluable assistance with material characterization and electrochemical measurements, respectively.

Conflicts of Interest

The authors declare no conflict of interest.

References

[1] Shrestha, D., 2024. Structural and electrochemical evaluation of renewable carbons and their composites on different carbonization temperatures for supercapacitor applications. Heliyon. 10(4), e25628. DOI: https://doi.org/10.1016/j.heliyon.2024.e25628

[2] Shrestha, D., 2023. Applications of functionalized

porous carbon from bio-waste of Alnus nepalensis in energy storage devices and industrial wastewater treatment. Heliyon. 9(11), e21804. DOI: https://doi.org/10.1016/j.heliyon.2023.e21804

[3] Shrestha, D., 2022a. Evaluation of Physical and Electrochemical Performances of Hardwood and Softwood derived Activated Carbon for Supercapacitor Application. Material Science for Energy Technology. 5, 353–365. DOI: https://doi.org/10.1016/j.mset.2022.09.002

[4] Shrestha, D., 2022b. Activated carbon and its hybrid composites with manganese (IV) oxide as effectual electrode materials for high performance supercapacitor. Arabian Journal of Chemistry. 15(7), 103946. DOI: https://doi.org/10.1016/j.arabjc.2022.103946

[5] Shrestha, D., Rajbhandari, A., 2021. The Effects of Different Activating Agents on the Physical and Electrochemical Properties of Activated Carbon Electrodes Fabricated from Wood-dust of Shorea robusta. Heliyon. 7(9), e07917. DOI: https://doi.org/10.1016/j.heliyon.2021.e07917

[6] Shrestha, D., Maensiri, S., Wongpratat, U., et al., 2019. Shorea robusta derived activated carbon decorated with manganese dioxide hybrid composite for improved capacitive behaviors. Journal of Environment Chemistry Engineering. 7(5), 103227. DOI: https://doi.org/10.1016/j.jece.2019.103227

[7] Shrestha, D., 2022c. Nanocomposite Electrode Materials Prepared from Pinus roxburghii and Hematite for Application in Supercapacitors. Journal of Korean Wood Science Technology. 50(4), 219–236. DOI: https://doi.org/10.5658/WOOD.2022.50.4.219

[8] Shrestha, D., Gyawali, G., Rajbhandari, A., 2018. Preparation and Characterization of Activated Carbon from Waste Sawdust from Saw Mill. Journal of Science and Technology. 22(2), 103–108. DOI: https://doi.org/10.3126/jist.v22i2.19600

[9] Yewale, M.A., Shin, D.K., Alam, W.M., et al., 2024. Controlled synthesis and electrochemical characterization of Co3V2O8 hexagonal sheets for energy storage applications. Colloids and Surfaces A: Physicochemical and Engineering Aspects. 703, 135180. DOI: https://doi.org/10.1016/j.colsurfa.2024.135180

[10] Desarada, S.V., Yewale, M., Vallabhapurapu, S., et al., 2024. Multiwalled carbon nanotube-cobalt vanadium oxide composite for high-performance supercapacitor electrodes with enhanced power density and cycling stability. Diamond and Related Materials. 149, 111557. DOI: https://doi.org/10.1016/j.diamond.2024.111557

[11] Yewale, M., Kumar, V., Teli, A., et al., 2024. Elevating Supercapacitor Performance of Co3O4-g-C3N4 Nanocomposites Fabricated via the Hydrothermal Method. Micromachines. 15(3), 414. DOI: https://doi.org/10.3390/mi15030414

[12] Rajivgandhi, P., Thirumal, V., Sekar, A., et al., 2025. Biomass-Derived Activated Porous Carbon from Foxtail Millet Husk to Utilizing High-Performance Symmetric Supercapacitor Applications. Nanomaterials. 15(8), 575. DOI: https://doi.org/10.3390/nano15080575

[13] Ping, L., Huanlei, W., 2021. Recent advances in carbon-supported iron group electrocatalysts for the oxygen reduction reaction. New Carbon Materials. 36(4), 665–682. DOI: https://doi.org/10.1016/S1872-5805(21)60072-0

[14] Yewale, M.A., Bharadwaj, V.S.L., Kadam, R.A., et al., 2024. Electrochemical study of CoV2O6 prepared by hydrothermal approach at different molar concentration of vanadium source. Materials Science and Engineering B. 307, 117464. DOI: https://doi.org/10.1016/j.mseb.2024.117464

[15] Zhang, M., Li, X., Wang, X., et al., 2020. Three-Dimensional Core-Branch α-Fe2O3@NiO/Carbon Cloth Heterostructured Electrodes for Flexible Supercapacitors. Frontiers in Chemistry. 7, 887. DOI: https://doi.org/10.3389/fchem.2019.00887

[16] Yewale, M.A., Teli, A.M., Beknalkar, S.A., et al., 2024. Smart Textile Flexible MnCo2O4 Electrodes: Urea Surface Modification for Improved Electrochemical Functionality. Materials. 17(8), 1866. DOI: https://doi.org/10.3390/ma17081866

[17] Gao, L., Liu, F., Qi, J., et al., 2025. Recent Advances and Challenges in Hybrid Supercapacitors Based on Metal Oxides and Carbons. Inorganics. 13(2), 49. DOI: https://doi.org/10.3390/inorganics13020049

[18] González-Banciella, A., Martinez-Diaz, D., Sánchez, M., et al., 2024. Nanostructured Transition Metal Oxides on Carbon Fibers for Supercapacitor and Li-Ion Battery Electrodes: An Overview. International Journal of Molecular Sciences. 25(15), 8514. DOI: https://doi.org/10.3390/ijms25158514

[19] Shen, H., Kong, X., Zhang, P., et al., 2021. In-situ hydrothermal synthesis of δ-MnO2/soybean pod carbon and its high performance application on supercapacitor. Journal of Alloys and Compounds. 853, 157357. DOI: https://doi.org/10.1016/j.jallcom.2020.157357

[20] Mehdipour-Ataei, S., Aram, E., 2023. Mesoporous Carbon-Based Materials: A Review of Synthesis, Modification, and Applications. Catalysts. 13(1), 2. DOI: https://doi.org/10.3390/catal13010002

[21] Wei, Z., Yanfei, Z., Jiao, W., 2025. Mesoporous carbon materials: synthesis methods, pro
perties, and advanced applications. Frontiers in Materials. 12, 1548671. DOI: https://doi.org/10.3389/fmats.2025.1548671

[22] Forouzandeh, P., Kumaravel, V., Pillai, S., 2020. Electrode Materials for Supercapacitors: A Review of Recent Advances. Catalysts. 10(9), 969. DOI: https://doi.org/10.3390/catal10090969

[23] Zhu, Y., Cheng, S., Zhou, W., et al., 2017. Porous Functionalized Self-Standing Carbon Fiber Paper Electrode for High Performance Capacitive Energy Storage. ACS Applied Materials & Interfaces. 9(15), 13173–13180. DOI: https://doi.org/10.1021/acsami.7b01210

[24] Geng, P., Zheng, S., Tang, H., et al., 2018. Transition metal sulfides based on graphene for electrochemical energy storage. Advanced Energy Materials. 8(15), 1703259. DOI: https://doi.org/10.1002/aenm.201703259

[25] Fan, J., Kang, L., Cheng, X., et al., 2022. Biomass-Derived Carbon Dots and Their Sensing Applications. Nanomaterials. 12(24), 4473. DOI: https://doi.org/10.3390/nano12244473

[26] Zhang, J., Yang, H., Huang, Z., et al., 2023. Pore-structure regulation and heteroatom doping of activated carbon for supercapacitors with excellent rate performance and power density. Waste Disposal & Sustainable Energy. 5(3), 417–426. DOI: https://doi.org/10.1007/s42768-023-00155-1

[27] Chakraborty, R., Pradhan, V.K.M., Nayak, A.K., 2022. Recent advancement of biomass-derived porous carbon based materials for energy and environmental remediation applications. Journal of Materials Chemistry A. 10(13), 6965–7005. DOI: https://doi.org/10.1039/D1TA10269A

[28] Sun, Y., Shi, X., Yang, Y., et al., 2022. Biomass-Derived Carbon for High-Performance Batteries: From Structure to Properties. Advanced Functional Materials. 32(24), 2201584. DOI: https://doi.org/10.1002/adfm.202201584

[29] Wang, G., Zhang, L., Zhang, J., 2012. A review of electrode materials for electrochemical supercapacitors. Chemical Society Reviews. 41(2), 797–828. DOI: https://doi.org/10.1039/C1CS15060J

[30] Lee, Y.S., Selvaraj, A.R., Kostoglou, N., et al., 2024. Asymmetric supercapacitors based on biomass-derived porous activated carbon (PAC)/1D manganese oxide (MnO2) electrodes with high power and energy densities. Materials Science and Engineering B. 304, 117368. DOI: https://doi.org/10.1016/j.mseb.2024.117368

[31] Mandal, S., Hu, J., Shi, S.Q., 2023. A comprehensive review of hybrid supercapacitor from transition metal and industrial crop based activated carbon for energy storage applications. Materials Today Communications. 34, 105207. DOI: https://doi.org/10.1016/j.mtcomm.2022.105207

[32] Liu, C., Li, F., Ma, L.P., et al., 2010. Advanced materials for energy storage. Advanced Materials. 22(8), E28–E62. DOI: https://doi.org/10.1002/adma.200903328

[33] Li, S., Tan, X., Li, H., et al., 2022. Investigation on pore structure regulation of activated carbon derived from sargassum and its application in supercapacitor. Scientific Reports. 12(1), 10106. DOI: https://doi.org/10.1038/s41598-022-14214-w

[34] Gan, Y.X.M., 2021. Activated Carbon from Biomass Sustainable Sources. C. 7(2), 39. DOI: https://doi.org/10.3390/c7020039

[35] Zhou, Q., Wu, M., Zhang, M., et al., 2017. Graphene-based electrochemical capacitors with integrated high-performance. Materials Today Energy. 6, 181–188. DOI: https://doi.org/10.1016/j.mtener.2017.09.015

[36] Shrestha, D., 2025. High-Performance Supercapacitor Electrodes from Optimized Single-Step Carbonized Michelia champaca Biomass. Journal of Environmental & Earth Sciences. 7(6), 1–22. DOI: https://doi.org/10.30564/jees.v7i6.8444

[37] Xu, B., Zheng, M., Tang, H., et al., 2019. Iron oxide-based nanomaterials for supercapacitors. Nanotechnology. 30(20), 204002. DOI: https://doi.org/10.1088/1361-6528/ab009f

[38] Obodo, R.M., Nwanya, A., Hassina, T., et al., 2020. Transition Metal Oxide-Based Nanomaterials for High Energy and Power Density Supercapacitor. In: Ezema, F. (ed.). Electrochemical Devices for Energy Storage Applications. CRC Press: Boca Raton, FL, USA. pp. 131–150.

[39] Arico, A.S., Bruce, P., Scrosati, B., et al., 2005. Nanostructured materials for advanced energy conversion and storage devices. Nature Materials. 4(5), 366–377. DOI: https://doi.org/10.1038/nmat1368

[40] Barsoukov, E., Macdonald, J.R., 2005. Impedance spectroscopy: theory, experiment, and applications, 2nd ed. Wiley: Hoboken, NJ, USA.

[41] Aricò, A.S., Bruce, P., Scrosati, B., et al., 2010. Nanostructured materials for advanced energy conversion and storage devices. In: Dusastre, V. (ed.). Materials For Sustainable Energy: A Collection Of Peer-reviewed Research And Review Articles From Nature Publishing Group. World Scientific Publishing Company: Singapore. pp. 148–159. DOI: https://doi.org/10.1142/9789814317665_0022

[42] Sun, G., Lin, H., Tian, R., et al., 2023. Rational design and synthesis of nanosheets self-assembled hierarchical flower-ball-like CuFeS2 for boosted wide temperature sodium-ion batteries. Nano Research. 16(7), 9407–9415. DOI: https://doi.org/10.1007/s12274-023-5614-1

[43] Fan, Z., Yan, J., Wei, F., et al., 2011. Asymmetric supercapacitors based on graphene/MnO2 and activated carbon nanofiber electrodes with high power and energy density. Advanced Functional Materials. 21(12), 2366–2375. DOI: https://doi.org/10.1002/adfm.201100058

[44] Xu, C., Kang, F., Du, B., 2010. Recent progress on manganese dioxide based supercapacitors. Journal of

Materials Research. 25, 1421–1432. DOI: https://doi.org/10.1557/JMR.2010.0211

[45] Julien, C.M., Mauger, A., 2017. Nanostructured MnO2 as Electrode Materials for Energy Storage. Nanomaterials. 7(11), 396. DOI: https://doi.org/10.3390/nano7110396

[46] Gao, H., Liu, S., Li, Y., et al., 2017. Critical Review of Spinel Structured Iron Cobalt Oxides Based Materials for Electrochemical Energy Storage and Conversion. Energies. 10(11), 1787. DOI: https://doi.org/10.3390/en10111787

[47] Liu, X., Chen, C., Zhao, Y., et al., 2013. A review on the synthesis of manganese oxide nanomaterials and their applications on lithium-ion batteries. Journal of Nanomaterials. 2013(1), 736375. DOI: https://doi.org/10.1155/2013/736375

[48] Ryoo, G., Kim, S., Lee, D., et al., 2024. Energy Storage Performance of Electrode Materials Derived from Manganese Metal–Organic Frameworks. Nanomaterials. 14(6), 503. DOI: https://doi.org/10.3390/nano14060503

[49] Zhang, X., Cheng, X., Zhang, Q., 2016. Nanostructured energy materials for electrochemical energy conversion and storage: a review. Journal of Energy Chemistry. 25(6), 967–984. DOI: https://doi.org/10.1016/j.jechem.2016.11.003

[50] Shrestha, D., 2024. Bio-based Acacia catechu/Ferric Oxide Nanostructured Composite Electrodes for Advanced Energy Storage Materials. Patan Pragya. 13(2), 22–37. DOI: https://doi.org/10.3126/pragya.v13i2.78781

[51] Lou, Z., Wang, Q., Kara, U., et al., 2021. Biomass-Derived Carbon Heterostructures Enable Environmentally Adaptive Wideband Electromagnetic Wave Absorbers. Nano-Micro Letters. 14(1), 11. DOI: https://doi.org/10.1007/s40820-021-00750-z

[52] Augustyn, V., Simon, P., Dunn, B., 2014. Pseudocapacitive oxide materials for high-rate electrochemical energy storage. Energy & Environmental Science. 7(5), 1597–1614. DOI: https://doi.org/10.1039/C3EE44164D

[53] Li, M., Tang, T.Z., Leng, M., et al., 2014. Flexible solid-state supercapacitor based on graphene-based hybrid films. Advanced Functional Materials. 24(47), 7495–7502. DOI: https://doi.org/10.1002/adfm.201402442

[54] Fischer, A.F., Pettigrew, K.A., Rolison, D.R., et al., 2007. Incorporation of homogeneous, nanoscale MnO2 within ultra-porous carbon structures via self-limiting electroless deposition: implications for electrochemical capacitors. Nano Letters. 7, 281–286. DOI: https://doi.org/10.1021/nl062263i

[55] Abdel Maksoud, M.I.A., Fahim, R.A., Shalan, A.E., et al., 2021. Advanced materials and technologies for supercapacitors used in energy conversion and storage: a review. Environmental Chemistry Letters. 19, 375–439. DOI: https://doi.org/10.1007/s10311-020-01075-w